

Conical Intersections and Geometric Phases in the Asymmetric Quantum Rabi Model

Zi-Min Li,¹ Devid Ferri,¹ David Tilbrook,¹ and Murray T. Batchelor^{1,2,3}

¹*Department of Theoretical Physics, Research School of Physics,
Australian National University, Canberra ACT, 2601, Australia*

²*Mathematical Sciences Institute, Australian National University, Canberra ACT, 2601, Australia*

³*Centre for Modern Physics, Chongqing University,
Chongqing 400044, The People's Republic of China*

(Dated: May 28, 2022)

Conical intersections (CIs) between energy surfaces arise in various physical contexts. A rich example, involving the interaction of a qubit with a bosonic field, is the energy landscape of the asymmetric quantum Rabi model (AQRM). Conventional approximations for this model, including the slow-qubit approximation, fail to capture the correct location of the CIs. To go beyond this limitation, we introduce a relatively simple solvable light-matter interaction model, which by construction, shares the same CIs as the AQRM. As a demonstration of the use of this simplified model we calculate the geometric phases around CIs in the energy landscape. We find that the geometric phases acquired by closed loops in parameter space around CIs are multiples of π , depending on the CIs encircled by the trajectories considered. These results are seen to be in agreement with numerical results for the corresponding geometric phases of the AQRM.

Introduction.— Following the pioneering work of Berry [1], geometric and topological aspects of quantum systems have been under intense investigation. Geometric phases and related topological phenomena have been identified and studied in many areas of physics, most notably in condensed-matter physics and optics [2–5]. The geometric phase also offers opportunities for quantum information and computation [4]. Here we consider geometric phases in a fundamental model of light-matter interaction – the quantum Rabi model (QRM) [6]. This model is realizable in terms of artificial atoms in quantum circuits [7–9]. The controlled accumulation of a geometric Berry phase in a superconducting charge qubit, manipulating the qubit geometrically using microwave radiation, and the associated accumulated phase has been demonstrated experimentally [10]. Measurements of the Berry phase in a superconducting charge pump have also been performed showing the dependence of both dynamic and geometric effects on the superconducting phase bias across the pump [11]. Measurements of a superconducting phase qubit have demonstrated a contribution from the second excited state to the two-level geometric phase in a weakly anharmonic but strongly driven two level system [12].

The geometric Berry phase [1] in the QRM has been discussed by several authors [5, 13, 14]. In that work the geometric phase is induced by a unitary transformation [15–19]. Further to the earlier experiment [10], a vacuum-induced Berry phase has been measured in the artificial atom interacting with the single microwave cavity mode [20]. The artificial atom acquires a geometric phase determined by the path traced out in the combined Hilbert space of the atom and the quantum field as the phase of the interaction is varied. Here we take a different approach and consider geometric phases associated with conical intersections (CIs) in the asymmetric quan-

tum Rabi model (AQRM). The AQRM is a deformation of the QRM in which the degeneracies in the energy spectrum of the QRM give rise to CIs in the energy spectrum of the AQRM. The energy landscape of the AQRM features an infinite number of CIs [21].

Our motivation is to calculate geometric phases around the Dirac-like cones induced by the CIs in the AQRM. In general it should be expected that the geometric phase is a multiple of π [1, 2]. In particular, the Herzberg/Longuet-Higgins theorem [22] implies that a two-level system with a real symmetric Hamiltonian always acquires a non-trivial π phase around a CI. We start from the slow-qubit approximation of the AQRM to give an analytic calculation of the geometric phases around CIs [3, 23] in the AQRM. Stepping beyond this approximation, we then propose a relatively simple exactly solved model that shares the same CIs and we argue, the same geometric phases, as the AQRM.

Energy landscape of the AQRM.— The AQRM is defined by the Hamiltonian ($\hbar = 1$)

$$H = \frac{\Delta}{2}\sigma_z + \omega a^\dagger a + g\sigma_x(a^\dagger + a) + \frac{\epsilon}{2}\sigma_x, \quad (1)$$

where σ_x and σ_z are Pauli matrices for a two-level system with level splitting Δ . The single mode bosonic field is described by the creation and annihilation operators a^\dagger and a , and frequency ω . The interaction between the two systems is via the coupling g . When $\epsilon = 0$, Eq. (1) reduces to the standard quantum Rabi model, which has \mathbb{Z}_2 parity symmetry [24]. Energy levels from different parity sectors are allowed to cross. In general, nonzero values of ϵ break this symmetry and the level crossings are avoided, leading to Dirac-like cones in the spectrum. In some special cases, where ϵ is a multiple of the field frequency ω , the two-fold degenerate level crossings reappear. This phenomenon, referred to as hidden symmetry

[25, 26], gives rise to additional CIs and rich topological properties. The commuting operators responsible for this hidden symmetry have recently been found [27], revealing an underlying Z_2 symmetry [27, 28]. A part of the energy landscape of the AQRM is displayed in Fig. 1, where several of the CIs are present.

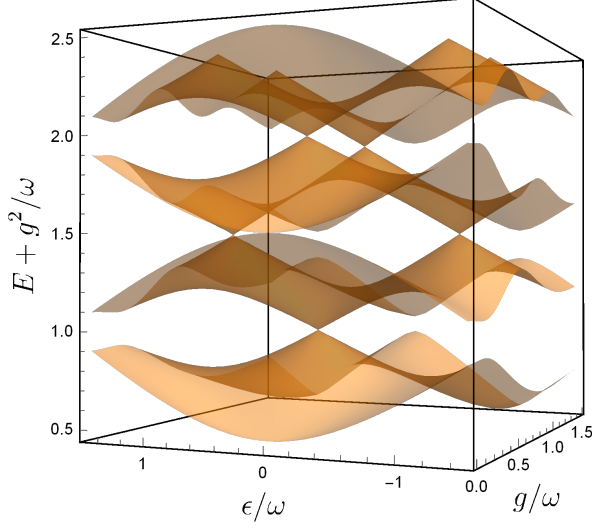


FIG. 1. Energy spectrum of the AQRM with respect to the parameters g and ϵ . Other parameter values are $\omega = 1$ and $\Delta = 1$. Conical intersections emerge only when ϵ takes integer values. For clarity, the lowest two levels are not shown and the energies are rescaled with $E + g^2/\omega$.

Slow-qubit approximation to the AQRM.— Although the analytic solution of the AQRM is known [29–32], it seems unlikely that it can be used to calculate the geometric properties of the AQRM analytically. For this reason we resort to some useful approximations. We first consider the limit $\Delta = 0$. In this case, Eq. (1) describes spin-dependent displaced oscillators [33, 34] and can be readily solved. The eigenstates and eigenvalues are

$$\begin{aligned} \psi_{n,\pm}^{\text{do}} &= |n_{\pm}, \pm\rangle = |n_{\pm}\rangle \otimes |\pm\rangle, \\ E_{n,\pm}^{\text{do}} &= n\omega - \frac{g^2}{\omega} \pm \frac{\epsilon}{2}, \end{aligned} \quad (2)$$

in which $|n_{\pm}\rangle = \exp[\pm g(a^\dagger - a)/\omega]|n\rangle$ are displaced Fock states, and $|\pm\rangle$ are the eigenstates of σ_x .

We now consider the case where $\Delta/\omega \ll 1$. Physically this means there is weak tunnelling between the two displaced oscillators. Without loss of generality, ϵ can be assumed to be non-negative since the AQRM is symmetric with regard to ϵ . The weak tunnelling induced by the Δ term only couples the state pairs $|n_+, +\rangle$ and $|(n+l)_-, -\rangle$, whereas the lowest l levels associated with the qubit state $|-\rangle$ stay uncoupled. Here $l = \lfloor \epsilon/\omega \rfloor$ is the integer closest to ϵ/ω [34]. This is known as the adiabatic or slow-qubit approximation (SQA) [33, 35], where “adiabatic” implies that the qubit transition is slow compared to the field frequency. As a consequence, Eq. (1) is

block-diagonal in the basis $\{|n_+, +\rangle, |(n+l)_-, -\rangle\}$, with the n th 2×2 matrix block described by

$$H_n^{\text{SQ}} = \left(n + \frac{l}{2}\right)\omega - \frac{g^2}{\omega} + \frac{\epsilon - l\omega}{2}\sigma_x^{(n)} + \frac{\Omega_{nl}}{2}\sigma_z^{(n)}. \quad (3)$$

Here the Pauli matrices are

$$\begin{aligned} \sigma_x^{(n)} &= |n_+, +\rangle\langle n_+, +| - |(n+l)_-, -\rangle\langle (n+l)_-, -|, \\ \sigma_z^{(n)} &= |n_+, +\rangle\langle (n+l)_-, -| + |(n+l)_-, -\rangle\langle n_+, +|, \end{aligned} \quad (4)$$

and the off-diagonal coupling terms are

$$\Omega_{nl} = \Delta \exp\left[-\frac{2g^2}{\omega^2}\right] \left(-\frac{2g}{\omega}\right)^l \sqrt{\frac{n!}{(n+l)!}} L_n^l\left(\frac{4g^2}{\omega^2}\right), \quad (5)$$

which are given in terms of the Laguerre polynomials L_n^l . It is then straightforward to obtain the eigenstates as

$$\begin{aligned} \psi_{n,+}^{\text{SQ}} &= \cos\frac{\theta_n}{2}|n_+, +\rangle + \sin\frac{\theta_n}{2}|(n+l)_-, -\rangle, \\ \psi_{n,-}^{\text{SQ}} &= -\sin\frac{\theta_n}{2}|n_+, +\rangle + \cos\frac{\theta_n}{2}|(n+l)_-, -\rangle, \end{aligned} \quad (6)$$

where θ_n is determined by

$$\tan\theta_n = \frac{\Omega_{nl}}{\epsilon - l\omega}. \quad (7)$$

The corresponding eigenvalues are then given as

$$E_{n,\pm}^{\text{SQ}} = \left(n + \frac{l}{2}\right)\omega - \frac{g^2}{\omega} \pm \frac{1}{2}\sqrt{\Omega_{nl}^2 + (\epsilon - l\omega)^2}. \quad (8)$$

Beyond the precondition $\Delta/\omega \ll 1$, these results work reasonably well when the condition $\sqrt{\Delta^2 + (\epsilon - l\omega)^2}/\omega \leq 1$ is satisfied. Most importantly, the level crossings only exist when ϵ/ω takes integer values, which is the key feature of the CIs in the AQRM. A comparison of the exact AQRM spectrum and that calculated from Eq. (8) is shown in Fig. 2(a). Also shown in Figs. 2(b) and 2(c) are the CIs produced by Eq. (8), with the exact result as a benchmark. The breakdown of the SQA beyond the above condition is further illustrated in the Supplemental Material [36].

Geometric phases around CIs.— With the simple analytic expressions at hand, we now turn to the calculation of the geometric phases around the CIs [37]. Suppose the system Hamiltonian $H(\mathbf{R})$ depends on the vector $\mathbf{R} = \{R_1, R_2, \dots, R_m\}$ of m real parameters. The stationary Schrödinger equation is then $H(\mathbf{R})|\psi_n(\mathbf{R})\rangle = E_n(\mathbf{R})|\psi_n(\mathbf{R})\rangle$. The most general form of the geometric phase is expressed as

$$\gamma_n = \oint_c \mathbf{A}(\mathbf{R}) \cdot d\mathbf{R}, \quad (9)$$

where the vector potential $\mathbf{A}(\mathbf{R}) = i\langle\psi_n(\mathbf{R})|\nabla_{\mathbf{R}}|\psi_n(\mathbf{R})\rangle$ is known as the Berry connection. In our case, we consider a two-dimensional parameter vector $\mathbf{R} = (g, \epsilon)$ since Δ and ω are conventionally fixed.

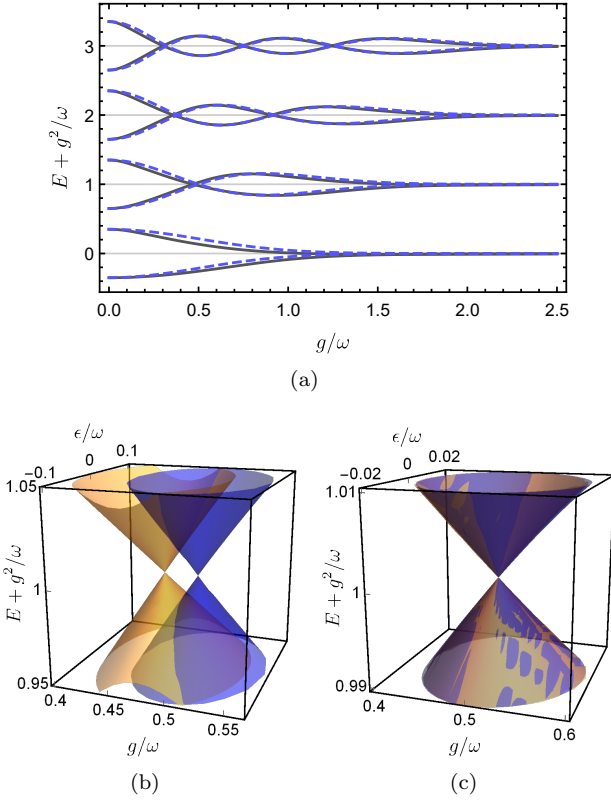


FIG. 2. (a) Energy spectrum of the AQRM obtained from exact diagonalization (solid lines) and from the slow-qubit approximation Eq. (8) (dashed lines). Other parameter values are $\epsilon = 0$, $\omega = 1$ and $\Delta = 0.7$. (b) The lowest conical intersection of the AQRM obtained through exact diagonalization (brown) and slow-qubit approximation (blue). The parameters are $\omega = 1$ and $\Delta = 0.7$. (c) The lowest conical intersection with the parameters $\omega = 1$ and $\Delta = 0.1$. For clarity the energies are rescaled with $E + g^2/\omega$.

By constructing the new basis

$$\begin{aligned} |\phi_n^+\rangle &= \frac{1}{\sqrt{2}} (|n_+, +\rangle + i|(n+l)_-, -\rangle), \\ |\phi_n^-\rangle &= \frac{1}{\sqrt{2}} (|n_+, +\rangle - i|(n+l)_-, -\rangle), \end{aligned} \quad (10)$$

the geometric phases for the n th pair of states are calculated as

$$\gamma_{\pm}^n = \mp m\pi. \quad (11)$$

Here the integer m is relevant to the configuration of degenerate points encircled by the parameter loop [3]. The geometric phases obtained in Eq. (11) only depend on the topological properties of the energy surfaces. Although Eq. (11) is derived with the SQA, the underlying physics is the same in the AQRM.

We now turn to numerical verification and further explore Eq. (11). As an illustrative example, we consider the 6th level of the AQRM, as shown in Fig. 2(a). The

corresponding energy surfaces, featuring the two CIs, are displayed in Fig. 3, on which we consider four trajectories. The blue ($g/\omega \in [0.2, 0.5], \epsilon/\omega \in [-0.1, 0.1]$) and green ($g/\omega \in [0.8, 1], \epsilon/\omega \in [-0.1, 0.1]$) trajectories each encircle a CI, whereas the red trajectory ($g/\omega \in [0.55, 0.7], \epsilon/\omega \in [-0.1, 0.1]$) does not. The large black loop ($g/\omega \in [0.25, 1.1], \epsilon/\omega \in [-0.15, 0.15]$) encircles the two CIs. Numerical calculations yield the corresponding geometric phases

$$\gamma^{\text{blue}} = \pi, \quad \gamma^{\text{green}} = -\pi, \quad \gamma^{\text{black}} = \gamma^{\text{red}} = 0, \quad (12)$$

each as expected [1, 2]. Importantly, the exact diagonalization of the AQRM in the appropriate basis also gives the same geometric phases and justifies the above derivations. Moreover, the above results remain valid for the AQRM beyond the validity of the SQA, which can be verified numerically. This is supported by the fact that all crossing points in the AQRM are doubly degenerate.

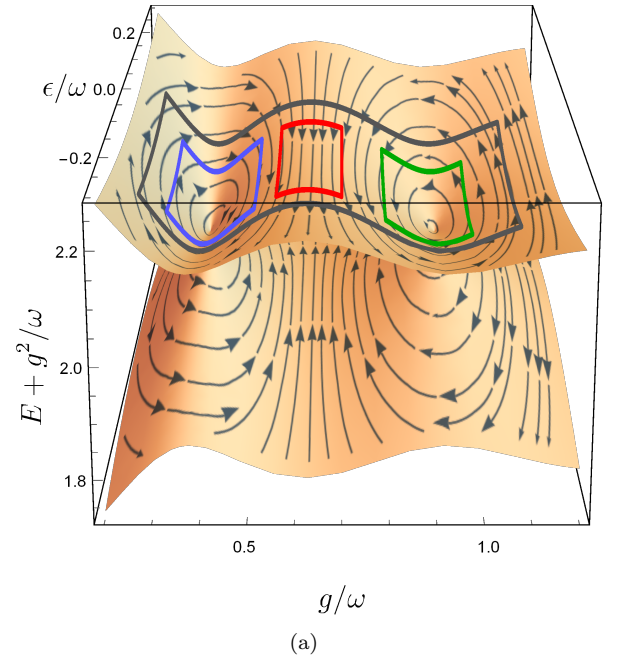


FIG. 3. Energy surfaces of the AQRM and the corresponding Berry connections under the SQA. The fixed parameters are $\Delta = 0.7$ and $\omega = 1$. We consider the four denoted trajectories (blue, red, green and black) in the (g, ϵ) parameter space. Here we have employed the gauge chosen in Eq. (S7) [36], which fixes the direction of flow.

Topological quantum Rabi model.— We have seen that, under the condition $\sqrt{\Delta^2 + (\epsilon - l\omega)^2}/\omega \leq 1$, the SQA provides simple analytic expressions to investigate the topological properties of the AQRM. Beyond this condition, the level crossings determined by Eq. (8) deviate from the exact results. The level crossings are known as Juddian points [38], which can be calculated through constraint polynomials of system parameters [31, 39–41]. Importantly, the Juddian points are exactly solvable for

arbitrary parameters. On the other hand, the crossing points predicted by Eq. (8) are determined through the zeros of Laguerre polynomials in Ω_{nl} , which are only exact in the limit $\Delta \rightarrow 0_+$. In the present case where only the degenerate points affect the geometric phases, we can replace Ω_{nl} with the corresponding constraint polynomials, such that the results Eq. (11) are exact for arbitrary system parameters.

We recall the recurrence relation [40]

$$\begin{aligned} P_0 &= 1, \quad P_1 = 4g^2 + \Delta^2/4 - \omega^2 - \epsilon\omega, \\ P_k &= (4kg^2 + \Delta^2/4 - k^2\omega^2 - k\epsilon\omega)P_{k-1} \\ &\quad - 4k(k-1)(n-k+1)g^2\omega^2P_{k-2}. \end{aligned} \quad (13)$$

The equation $P_n = 0$ then defines the constraint polynomials determining the degenerate points of the n th pair of levels in the AQRM. When $\Delta = 0$, the constraint polynomials reduce to the corresponding Laguerre polynomials in Eq. (8), which justifies the fact that the SQA is only exact in the limit $\Delta \rightarrow 0_+$. From the constraint polynomials, the number of degenerate points on each level and for each value of ϵ is also known [25, 40]. In other words, all necessary information determining the topological properties of the AQRM is exactly known. Furthermore, the CIs, determined by the constraint polynomials, are the sources of Berry curvature and thus the geometric phases [36].

To this end, we are now able to construct a simple solvable model that shares the same CIs as the AQRM by replacing the “topologically-inaccurate” part in the SQA with its exact counterpart. For this purpose, because the constraint polynomials can be very large for some parameters, we need to bound their range to avoid unphysical crossings in the spectrum. By doing so we have the eigenvalues

$$E_{n,\pm}^{\text{TQRM}} = \left(n + \frac{l}{2}\right)\omega - \frac{g^2}{\omega} \pm \frac{1}{2}\sqrt{K_n^2 + (\epsilon - l\omega)^2}, \quad (14)$$

where K_n are the bounded functions sharing the same roots with the constraint polynomials. Here K_n are chosen as

$$K_n = \frac{1}{2} \arctan \left[\frac{P_n}{(n+1)^2} \right]. \quad (15)$$

Note that the way to bound P_n is not unique. For example, other choices can be made to provide a more accurate regular spectrum.

We refer to this simplified model as the topological quantum Rabi model (TQRM), described by the Hamiltonian

$$H_n^{\text{TQRM}} = \left(n + \frac{l}{2}\right)\omega - \frac{g^2}{\omega} + \frac{1}{2}(\epsilon - l\omega)\sigma_x^{(n)} + \frac{1}{2}K_n\sigma_z^{(n)}, \quad (16)$$

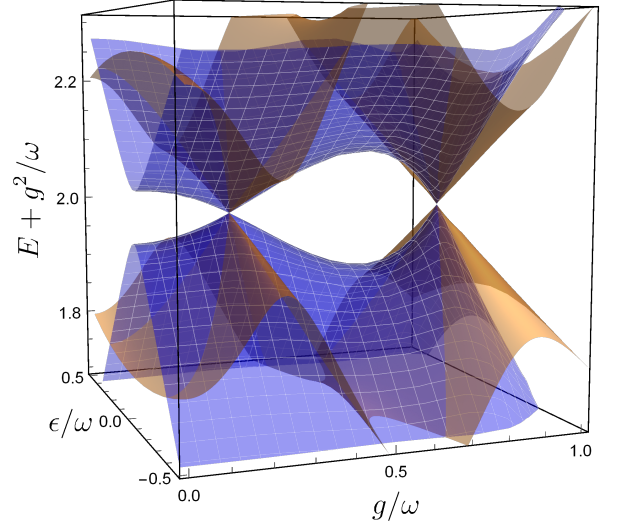


FIG. 4. The 5th and 6th energy surfaces of the AQRM (brown) and the TQRM Eq. (16) (blue with mesh). Parameter values are $\Delta/\omega = 1.5$. For clarity, the lowest two levels are not shown and the energies are rescaled with $E + g^2/\omega$.

where $\sigma_{x,z}^{(n)}$ are the same as Eq. (4). The eigenstates take the form

$$\begin{aligned} |\psi_{n,+}^{\text{TQRM}}\rangle &= \frac{1}{\sqrt{2}} (|\phi_n^+\rangle + e^{i\alpha}|\phi_n^-\rangle), \\ |\psi_{n,-}^{\text{TQRM}}\rangle &= \frac{1}{\sqrt{2}} (-e^{-i\alpha}|\phi_n^+\rangle + |\phi_n^-\rangle), \end{aligned} \quad (17)$$

with α determined by

$$\tan \alpha = \frac{K_n}{\epsilon - l\omega}. \quad (18)$$

The spectrum of the TQRM Hamiltonian (16) is compared with that of the AQRM in Fig. 4, where, by construction, the CI points are exactly equivalent [42]. The corresponding geometric phases are also exactly calculated. With Eqs. (17) and (18), we can calculate the geometric phases in the AQRM exactly for any trajectories and arbitrary parameter values.

This TQRM approach can be readily applied to other light-matter interaction models, such as the anisotropic Rabi model and the Rabi-Stark model, where the hidden symmetry is also present and the Juddian points therein are exactly solvable. An even more interesting phenomenon in these two models is that a parameter-dependent conical intersection occurs in the ground state, for which topological transitions can be explored analytically within the framework of our TQRM.

Conclusion.— In summary, by generalizing the SQA to the AQRM, we have investigated the topological properties around the CIs in the energy landscape of the AQRM. The geometric phases are always multiples of π , with the precise multiple depending on the configuration of CIs encircled by the trajectories considered. To

overcome the limitations of the SQA in approximating the energy landscape of the AQRM, we have proposed a relatively simple solvable Hamiltonian (16) based on the exact solution for the degenerate points in the AQRM. This TQRM shares the same CIs and geometric phases and makes it possible to explore the topological properties of the AQRM both analytically and exactly.

It remains to be seen if the geometric phases of the AQRM can be explored and measured in the context of cQED experiments where the asymmetric bias term appears naturally. In particular, the most accessible cones in the AQRM energy spectrum are within the deep strong coupling regime reached in recent experiments [43, 44]. It would also be very interesting to explore the possible cQED realisation of the simpler TQRM.

The authors thank the referees for their careful reading of the manuscript and insightful observations. This work is supported by the Australian Research Council grants DP170104934 and DP180101040.

-
- [1] M. V. Berry, *Proc. R. Soc. A* **392**, 45 (1984).
 - [2] A. Shapere and F. Wilczek, *Geometric Phases in Physics* (World Scientific, Singapore, 1989).
 - [3] A. Böhm, A. Mostafazadeh, H. Koizumi, Q. Niu, and J. Zwanziger, *The Geometric Phase in Quantum Systems* (Springer Berlin Heidelberg, 2003).
 - [4] E. Cohen, H. Larocque, F. Bouchard, F. Nejdassattari, Y. Gefen, and E. Karimi, *Nature Reviews Physics* **1**, 437 (2019).
 - [5] J. Larson, E. Sjöqvist, and P. Öhberg, *Conical Intersections in Physics* (Springer-Verlag GmbH, 2020).
 - [6] I. I. Rabi, *Phys. Rev.* **49**, 324 (1936); *Phys. Rev.* **51**, 652 (1937).
 - [7] A. F. Kockum, A. Miranowicz, S. D. Liberato, S. Savasta, and F. Nori, *Nat. Rev. Phys.* **1**, 19 (2019).
 - [8] P. Forn-Díaz, L. Lamata, E. Rico, J. Kono, and E. Solano, *Rev. Mod. Phys.* **91**, 025005 (2019).
 - [9] A. Blais, A. L. Grimsmo, S. M. Girvin, and A. Wallraff, (2020), [arXiv:2005.12667 \[quant-ph\]](#).
 - [10] P. J. Leek, J. M. Fink, A. Blais, R. Bianchetti, M. Göppl, J. M. Gambetta, D. I. Schuster, L. Frunzio, R. J. Schoelkopf, and A. Wallraff, *Science* **318**, 1889 (2007).
 - [11] M. Möttönen, J. J. Vartiainen, and J. P. Pekola, *Phys. Rev. Lett.* **100**, 177201 (2008).
 - [12] S. Berger, M. Pechal, S. Pugnetti, A. A. Abdumalikov, L. Steffen, A. Fedorov, A. Wallraff, and S. Filipp, *Phys. Rev. B* **85**, 220502 (2012).
 - [13] I. Fuentes-Guridi, A. Carollo, S. Bose, and V. Vedral, *Phys. Rev. Lett.* **89**, 220404 (2002).
 - [14] J. Larson, *Phys. Rev. Lett.* **108**, 033601 (2012).
 - [15] W.-W. Deng and G.-X. Li, *J. Phys. B: At., Mol. Opt. Phys.* **46**, 224018 (2013).
 - [16] M. Wang, L. Wei, and J. Liang, *Phys. Lett. A* **379**, 1087 (2015).
 - [17] L. Mao, S. Huai, L. Guo, and Y. Zhang, *Ann. Phys.* **362**, 538 (2015).
 - [18] J. Calderón and F. De Zela, *Phys. Rev. A* **93**, 033823 (2016).
 - [19] Y. Wang and X. Luo, *Opt. Commun.* **451**, 13 (2019).
 - [20] S. Gasparinetti, S. Berger, A. A. Abdumalikov, M. Pechal, S. Filipp, and A. Wallraff, *Science Advances* **2**, e1501732 (2016).
 - [21] M. T. Batchelor, Z.-M. Li, and H.-Q. Zhou, *J. Phys. A: Math. Theor.* **49**, 01LT01 (2016).
 - [22] G. Herzberg and H. C. Longuet-Higgins, *Disc. Faraday Soc.* **35**, 77 (1963).
 - [23] A. A. Mailybaev, O. N. Kirillov, and A. P. Seyranian, *Dokl. Math.* **73**, 129 (2006).
 - [24] D. Braak, *Symmetry* **11**, 1259 (2019).
 - [25] M. Wakayama, *J. Phys. A: Math. Theor.* **50**, 174001 (2017).
 - [26] S. Ashhab, *Phys. Rev. A* **101**, 023808 (2020).
 - [27] V. V. Mangazeev, M. T. Batchelor, and V. V. Bazhanov, *J. Phys. A: Math. Theor.* **54**, 12LT01 (2021).
 - [28] C. Reyes-Bustos, D. Braak, and M. Wakayama, (2021), [arXiv:2101.04305 \[math-ph\]](#).
 - [29] D. Braak, *Phys. Rev. Lett.* **107**, 100401 (2011).
 - [30] Q.-H. Chen, C. Wang, S. He, T. Liu, and K.-L. Wang, *Phys. Rev. A* **86**, 023822 (2012).
 - [31] H. Zhong, Q. Xie, X. Guan, M. T. Batchelor, K. Gao, and C. Lee, *J. Phys. A: Math. Theor.* **47**, 045301 (2014).
 - [32] A. J. Maciejewski, M. Przybylska, and T. Stachowiak, *Phys. Lett. A* **378**, 3445 (2014).
 - [33] E. K. Irish, J. Gea-Banacloche, I. Martin, and K. C. Schwab, *Phys. Rev. B* **72**, 195410 (2005).
 - [34] Z.-M. Li and M. T. Batchelor, *Phys. Rev. A* **103**, 023719 (2021).
 - [35] J. Semple and M. Kollar, *J. Phys. A: Math. Theor.* **51**, 044002 (2017).
 - [36] See Supplemental Material at [URL to be inserted by publisher].
 - [37] The necessary background and details are given in the Supplemental Material [36].
 - [38] B. R. Judd, *J. Phys. C: Solid State Phys.* **12**, 1685 (1979).
 - [39] M. Kuś, *J. Math. Phys.* **26**, 2792 (1985).
 - [40] Z.-M. Li and M. T. Batchelor, *J. Phys. A: Math. Theor.* **48**, 454005 (2015); *J. Phys. A: Math. Theor.* **49**, 369401 (2016).
 - [41] K. Kimoto, C. Reyes-Bustos, and M. Wakayama, *Int. Math. Res. Not.* (2020), 10.1093/imrn/rnaa034.
 - [42] Further comparisons between the TQRM and the AQRM are given in the Supplemental Material [36].
 - [43] F. Yoshihara, T. Fuse, S. Ashhab, K. Kakuyanagi, S. Saito, and K. Semba, *Nat. Phys.* **13**, 44 (2016).
 - [44] F. Yoshihara, T. Fuse, Z. Ao, S. Ashhab, K. Kakuyanagi, S. Saito, T. Aoki, K. Koshino, and K. Semba, *Phys. Rev. Lett.* **120**, 183601 (2018).

Supplemental Material: Conical Intersections and Geometric Phases in the Asymmetric Quantum Rabi Model

I. CALCULATING THE GEOMETRIC PHASES WITH SLOW-QUBIT APPROXIMATION

Suppose the system Hamiltonian $H(\mathbf{R})$ depends on the vector $\mathbf{R} = \{R_1, R_2, \dots, R_m\}$ of m real parameters. According to the adiabatic approximation, if the system is initially in an eigenstate, and the parameters \mathbf{R} are varied slowly enough, the system will stay in the eigenstate corresponding to the Hamiltonian with the instantaneous parameters \mathbf{R} . The stationary Schrödinger equation is then

$$H(\mathbf{R})|\psi_n(\mathbf{R})\rangle = E_n(\mathbf{R})|\psi_n(\mathbf{R})\rangle. \quad (\text{S1})$$

If we consider the time evolution of the system, the time-dependent Schrödinger equation gives rise to a regular dynamical phase that depends on the evolution time period, and a geometric phase that only depends on the path taken in the parameter space. For a closed path \mathcal{C} in parameter space, the general form of the geometric phase is

$$\gamma_n = \oint_{\mathcal{C}} \mathbf{A}_n(\mathbf{R}) \cdot d\mathbf{R}, \quad (\text{S2})$$

where the vector potential

$$\mathbf{A}_n(\mathbf{R}) = i \langle \psi_n(\mathbf{R}) | \nabla_{\mathbf{R}} | \psi_n(\mathbf{R}) \rangle \quad (\text{S3})$$

is known as the Berry connection in parameter space.

We now calculate the geometric phases in the AQRM under slow-qubit approximation. In our case, we consider a two-dimensional parameter space with the vector $\mathbf{R} = (g, \epsilon)$ since Δ and ω are conventionally fixed. Since the geometric phase vanishes for real eigenvectors, we need to introduce some imaginary factors in the system [S1, S2]. From the slow-qubit basis $\{|n_+, +\rangle, |(n+l)_-, -\rangle\}$, we construct a new basis

$$|\phi_n^+\rangle = \frac{1}{\sqrt{2}} (|n_+, +\rangle + i|(n+l)_-, -\rangle), \quad |\phi_n^-\rangle = \frac{1}{\sqrt{2}} (|n_+, +\rangle - i|(n+l)_-, -\rangle). \quad (\text{S4})$$

The 2×2 matrix block Eq. (3) in the main text is rewritten in this basis as

$$H'_n = \begin{pmatrix} h_{11} & h_{12} \\ h_{21} & h_{22} \end{pmatrix}, \quad (\text{S5})$$

with

$$h_{11} = h_{22} = \left(n + \frac{l}{2}\right) \omega - \frac{g^2}{\omega}, \quad h_{12} = h_{21}^* = \frac{1}{2}(\epsilon - l\omega) - \frac{i}{2}\Omega_{nl}. \quad (\text{S6})$$

The eigenvalues remain unchanged, as in Eq. (8) in the main text, whereas the eigenstates are now

$$|\psi_n^+\rangle = \frac{1}{\sqrt{2}} (|\phi_n^+\rangle + e^{i\theta_n} |\phi_n^-\rangle), \quad |\psi_n^-\rangle = \frac{1}{\sqrt{2}} (-e^{-i\theta_n} |\phi_n^+\rangle + |\phi_n^-\rangle), \quad (\text{S7})$$

in which θ_n is again determined through Eq. (7) in the main text. More generally, the eigenvalues remain unchanged with respect to additional multiplicative factors of $e^{\pm i\theta_n}$, which constitutes a gauge freedom. Throughout this work we have employed the gauge given by Eq. (S7).

Having obtained the wavefunctions, we can compute the corresponding geometric phases. We consider a loop in the two-dimensional parameter space (g, ϵ) with fixed $\Delta \leq 1$. The change in θ_n must be a multiple of 2π , i.e.,

$$\theta_n^f - \theta_n^i = 2m\pi, \quad m \in \mathbb{Z}, \quad (\text{S8})$$

where θ_n^i and θ_n^f are the initial and final values of θ_n , respectively. The geometric phases for the n th pair of states are then calculated as

$$\gamma_{\pm}^n = i \oint_{\mathcal{C}} \left\langle \psi_n^{\pm} \left| \frac{d\theta_n}{d\mathbf{R}} \frac{d}{d\theta_n} \right| \psi_n^{\pm} \right\rangle \cdot d\mathbf{R} = \mp m\pi. \quad (\text{S9})$$

Here the integer m is relevant to the configuration of degenerate points encircled by the parameter loop [S1]. In other words, the geometric phases obtained in Eq. (S9) are topological in the sense that they cannot vary smoothly.

II. CONICAL INTERSECTIONS ARE THE SOURCES OF BERRY CURVATURE

It is always helpful to consider the analogies between geometric quantities in parameter space and the magnetic quantities in real space. Specifically, the Berry connection (S3) is analogous to the magnetic vector potential since they depend on gauge choice in the same manner. Analogously, a Berry “field” can be defined by taking the curl of the Berry connection,

$$\mathbf{B}_n(\mathbf{R}) = \nabla \times \mathbf{A}_n(\mathbf{R}). \quad (\text{S10})$$

By Stokes’ theorem, geometric phases can then be calculated through Berry curvature,

$$\gamma_n = \iint_S \mathbf{B}_n(\mathbf{R}) \cdot d\mathbf{S}, \quad (\text{S11})$$

where S is the area enclosed by the path \mathcal{C} in parameter space. Eq. (S11) signifies the analogy between geometric phase and magnetic flux.

Eq. (S10) yields

$$\mathbf{B}_n = -\text{Im} \langle \nabla \psi_n | \times | \nabla \psi_n \rangle. \quad (\text{S12})$$

Inserting the complete set of instantaneous basis states, we then have

$$\mathbf{B}_n = -\text{Im} \sum_{m \neq n} \langle \nabla \psi_n | \psi_m \rangle \times \langle \psi_m | \nabla \psi_n \rangle. \quad (\text{S13})$$

Here the term with $m = n$ has been omitted since it has no imaginary part. To find $\langle \nabla \psi_n | \psi_m \rangle$, we take the gradient of the time independent Schrödinger equation (S1) and project onto $|\psi_m\rangle$. This yields

$$\langle \psi_m | \nabla H | \psi_n \rangle + \langle \psi_m | H | \nabla \psi_n \rangle = \langle \psi_m | \nabla E_n | \psi_n \rangle + \langle \psi_m | E_n | \nabla \psi_n \rangle. \quad (\text{S14})$$

With $\langle \psi_m | H = E_m \langle \psi_m |$, we obtain

$$\langle \psi_m | \nabla \psi_n \rangle = \frac{\langle \psi_m | \nabla H | \psi_n \rangle}{E_m - E_n}, \quad m \neq n. \quad (\text{S15})$$

Substituting back into Eq. (S13) leads to the expression

$$\mathbf{B}_n = -\text{Im} \sum_{m \neq n} \frac{\langle \psi_m | \nabla H | \psi_n \rangle \times \langle \psi_n | \nabla H | \psi_m \rangle}{(E_n - E_m)^2} \quad (\text{S16})$$

for Berry curvature. This equation tells us that the Berry curvature is singular at degenerate points. In fact, it can be shown that the sources of Berry curvature in parameter space are analogous to magnetic monopoles in magnetism.

III. GEOMETRIC PHASES BEYOND SLOW-QUBIT APPROXIMATION

In the main text we employ the slow-qubit approximation (SQA) to reduce the AQRM Hamiltonian into block diagonalized form consisting of infinitely many 2×2 matrices, which can be easily solved. Then the geometric phases around CIs in AQRM are calculated under the SQA, as shown in the preceding section. In fact, as long as the CIs are doubly degenerate and the Hamiltonian is real, the geometric phases are multiples of π .

As mentioned in the main text, the SQA is only valid for $\sqrt{\Delta^2 + (\epsilon - l\omega)^2}/\omega \leq 1$. In Fig. S1(c), it is shown that unphysical level crossings emerge in the energy spectrum of the SQA beyond its validity. These unphysical crossings drastically change the geometry of the model as the resulting CIs are the sources of geometric phases. In Fig. S1 we also see that the real level crossings predicted by SQA deviate substantially from the exact AQRM, and the deviations grow with Δ .

Here we numerically calculate the geometric phases in the AQRM beyond the validity of the SQA. As an illustrative example, we take $\Delta/\omega = 1.5$. We consider four trajectories similar to those in Fig. 3 of the main text and calculate the geometric phases. As expected, the geometric phases around closed trajectories are always multiples of π , depending on the number of CIs enclosed. The only difference lies in the positions of the CIs. This is not surprising since it can be seen from the constraint polynomials in the main text that the positions of the CIs depend on all system parameters.

IV. COMPARISON BETWEEN TQRM AND AQRM

Specifically, there are two important limitations in SQA. Firstly, when the predicted locations of level crossings are not accurate. Secondly, the SQA is invalid for $\Delta/\omega > 1$ due to the unphysical level crossings.

Now that we have numerically shown that in the case beyond SQA, the geometric phases in the AQRM behave the same, with the only difference being the positions of the CIs, it is then natural to attempt to modify the SQA to improve its performance.

Fortunately, the above two issues can be perfectly dealt with by the proposed TQRM Hamiltonian. The level crossings of the TQRM are predicted by the exactly solved constraint polynomials of system parameters. Therefore, the level crossings of the TQRM are always exact. On the other hand, by construction, the energy levels are normalized such that there are no extra unphysical level crossings. In other words, the TQRM has exactly the same CIs in the whole parameter space, two examples of which are displayed in Fig. S2, with $\Delta/\omega = 1$ and $\Delta/\omega = 1.5$, respectively. In the preceding section it is shown that CIs act as sources of Berry curvature and thus geometric phases. As a consequence, an arbitrary trajectory in parameter space gives the same geometric phases in the TQRM and the AQRM.

-
- [S1] A. Böhm, A. Mostafazadeh, H. Koizumi, Q. Niu and J. Zwanziger, *The Geometric Phase in Quantum Systems* (Springer Berlin Heidelberg, 2003).
[S2] A. A. Mailybaev, O. N. Kirillov and A. P. Seyranian, *Dokl. Math.* **73**, 129 (2006)

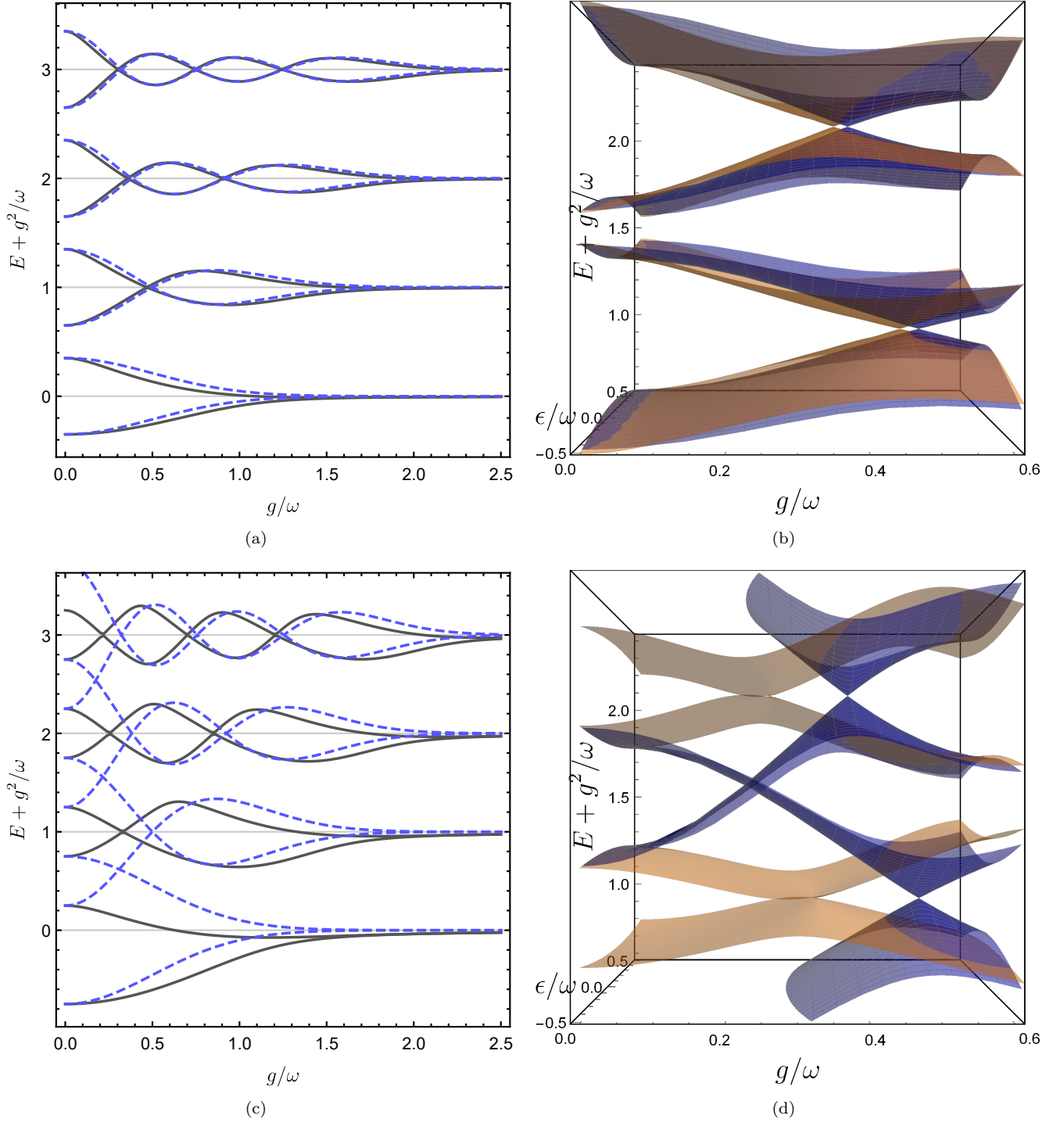


FIG. S1. (a)(c) Energy spectrum of the AQRM obtained from exact diagonalization (solid lines) and from the SQA Eq. (8) (dashed lines) with (a) $\Delta/\omega = 0.7$, (c) $\Delta/\omega = 1.5$ and $\epsilon = 0$ in both figures. The corresponding energy surfaces with varying ϵ/ω for comparison with (b) $\Delta/\omega = 0.7$ and (d) $\Delta/\omega = 1.5$.

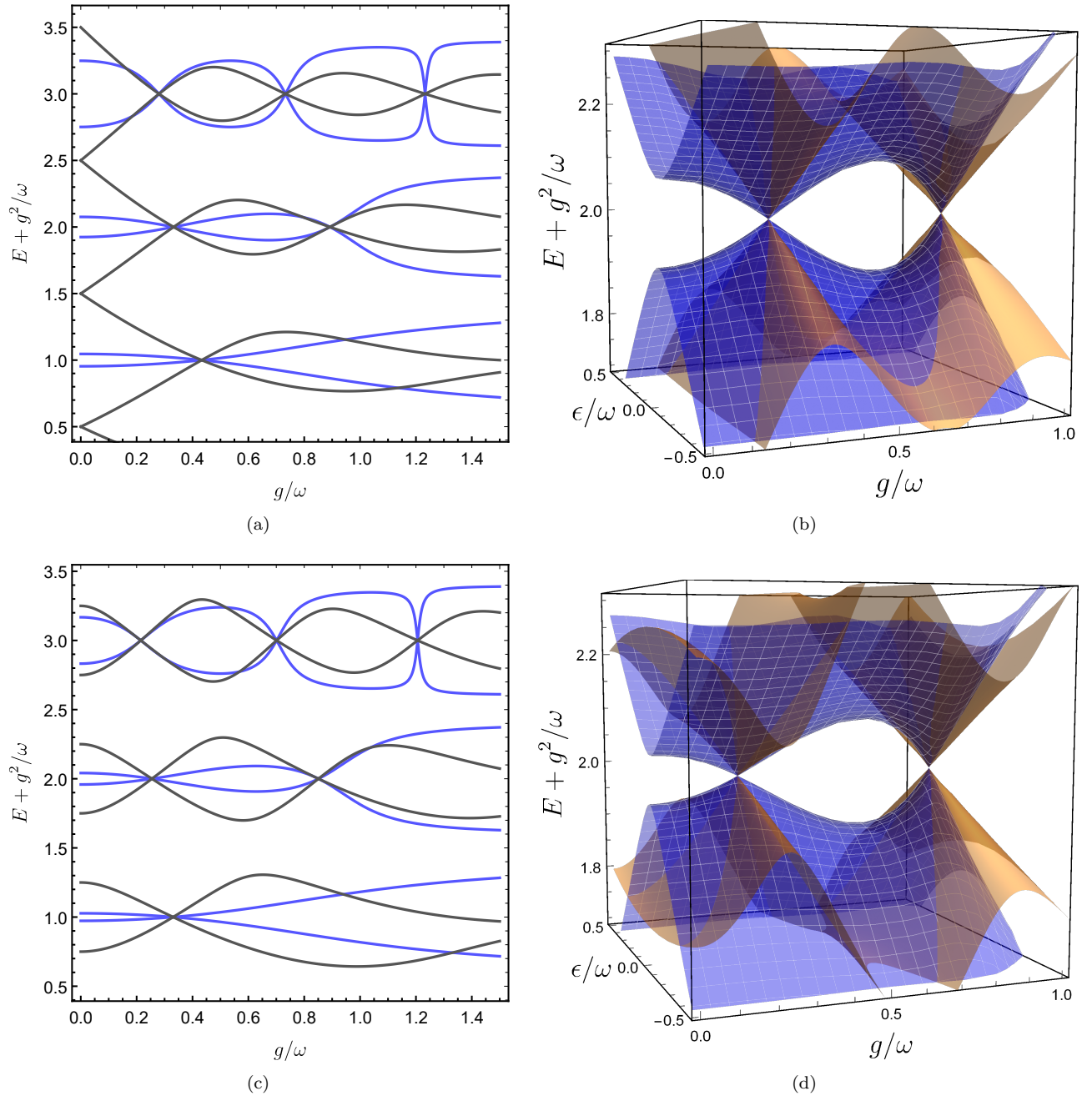


FIG. S2. Energy spectra of the AQRM (brown) and the TQRM (blue). The parameter values are $\omega = 1$ and (a) $\Delta = 1, \epsilon = 0$, (b) $\Delta = 1$, (c) $\Delta = 1.5, \epsilon = 0$, (d) $\Delta = 1.5$. By construction, the two models share the same CI's and geometric phases.